AIAA 80-1389R

Airfoil Flow Analysis with a Special Solution for Shock/Boundary-Layer Interaction

M. Nandanan* and E. Stanewsky†
Deutsche Forschungs - und Versuchsanstalt für Luft - und Raumfahrt e.V.
Aerodynamische Versuchsanstalt Göttingen, Göttingen, FRG
and
G. R. Inger‡
Virginia Polytechnic Institute and State University, Blacksburg, Va.

Shock/boundary-layer interaction has a crucial effect on transonic airfoil flow because it governs the way the boundary layer responds to the subsequent adverse pressure gradients thereby influencing the flow conditions at the trailing edge. It seems, therefore, important to incorporate a detailed and physically correct treatment of the interaction in the overall flowfield analysis. In the present approach, which is limited to nonseparating turbulent flow, this is accomplished by imbedding an analytical solution for near-normal shock/boundary-layer interaction as a module within a boundary-layer/inviscid flow computation code. This paper briefly describes the components involved in the present method and their coupling and compares theoretical results with results from boundary layer and surface pressure measurements carried out on three supercritical airfoils. The comparisons emphasize the need for the correct treatment of shock/boundary-layer interaction in transonic airfoil flow.

Nomenclature

a = speed of sound
c = airfoil chord
c_D = dissipation coefficient
c_f = skin friction coefficient
C_L = lift coefficient
c_p = pressure coefficient, $(p-p_\infty)/q_\infty$
H = shape factor, δ^*/Θ
$\bar{H}$ = Θ^*/Θ
M = local Mach number
M_∞ = freestream Mach number
$M_{\infty c}$ = corrected freestream Mach number
p = static pressure
q = dynamic pressure
Re = Reynolds number based on freestream conditions and chord
$Re_{\delta_1^*}$ = local Reynolds number based on δ_1^*
U_e = velocity at the edge of the boundary layer
u,v = velocity component in x and y, respectively
x,y = rectangular coordinates
x/c = nondimensional chord
α,α_g = corrected and geometric angle of attack, respectively
γ = ratio of specific heats
δ = boundary-layer thickness
δ^* = displacement thickness
Θ = momentum thickness, shock angle
Θ^* = energy thickness
ρ = density
Φ = velocity potential

Subscripts

B = boundary layer
e = edge of boundary layer
i = incompressible
1 = upstream of shock
∞ = freestream conditions

Presented as Paper 80-1389 at the AIAA 13th Fluid and Plasma Dynamics Conference, Snowmass, Colo., July 14-16, 1980; submitted Sept. 18, 1980; revision received May 20, 1981. Copyright © American Institute of Aeronautics and Astronautics, Inc., 1980. All rights reserved.

*Research Scientist, National Aeronautical Laboratory, Bangalore, India (on deputation to DFVLR).
†Research Scientist. Member AIAA.
‡Professor of Aerospace and Ocean Engineering. Associate Fellow AIAA.

Introduction

TRANSONIC airfoil flow is to a large degree affected by viscous-inviscid interactions. Among them, a key role is played by 1) the interaction of the boundary layer with the shock wave imbedded in the flowfield, mainly of concern under off-design conditions and 2) the interaction of the boundary layer with the sustained adverse pressure gradients close to the trailing edge on the airfoil upper surface. The importance of viscous effects to airfoil (and wing) design is best demonstrated by the fact that the best design is probably the one which decelerates the flow from the high velocities that provide the lift to the maximum pressure recovery at the trailing edge without separating the flow or excessively thickening the boundary layer; the more rapidly this deceleration can be performed the greater the extent of the surface over which the lift can be maintained.

The significance of transonic flow in general and the interaction phenomena in particular has led to extensive experimental and theoretical research in industry and research organizations. Considering theoretical methods one may roughly distinguish the following concepts.[1]

1) Viscous flow analysis is carried out by coupling the outer inviscid flow and the dissipative layer via the displacement thickness, the latter determined in a first approximation by boundary-layer theory.

2) The time-averaged Navier-Stokes equations are solved. This approach, although very costly, is probably the best, especially in the presence of large separated regions.

3) One may compromise by employing the concept 1 in certain domains and use in areas of strong interactions such as the shock impingement and trailing edge domains a solution of the Navier-Stokes equations or approximations to these solutions as provided, e.g., by multiple deck theory.

In shock/boundary interactions the physics of the flow are not well represented by boundary-layer theory. It is, therefore, very unlikely that boundary-layer theory can predict changes in the boundary-layer properties such as the displacement thickness, the shape factor, and the skin friction with sufficient accuracy even if artificial means such as

smearing of the pressure rise due to the shock are introduced. A high accuracy of the data immediately downstream of the shock seems, however, to be required since small errors here may be amplified in the subsequent computation and carried to the trailing edge. Experimental evidence of the magnification of small differences downstream of the shock by the subsequent sustained adverse pressure gradients is reported in Ref. 1.

Evidence exists[2] that conventional boundary-layer methods also fail to account for strong interaction effects that occur near the trailing edge and in the near wake behind the airfoil.

In the present approach to transonic airfoil flow analysis, modeled after concept 1, shock/boundary-layer interaction is accounted for by imbedding an analytical solution for near-normal shock wave/boundary-layer interaction in a module within a boundary-layer/inviscid computation code. No special solution for the trailing edge interaction is provided. However, the inviscid code employed models the wake, although rather crudely, as a semi-infinite parallel displacement body extending downstream of the trailing edge.

In the following sections the components of the overall method and their coupling are described briefly. Subsequently, theoretical results are compared to data from boundary layer and surface pressure measurements carried out on three supercritical airfoils. It will be shown that it is necessary to treat shock/boundary-layer interaction in a physically correct way in order to accurately predict the boundary-layer development over the rear part of the airfoil.

Theory

The components comprising the present method are an inviscid computation code, a boundary-layer code and a shock/boundary-layer interaction code. The viscous flow analysis is carried out by applying the displacement surface concept.

Inviscid Flow Theory

For the inviscid computation of the flow about the effective airfoil contour Jameson's version[3] of the relaxation method of Bauer et al.[4] is employed. The code provides options to either solve the quasilinear equation for the velocity potential

$$(a^2-u^2)\Phi_{xx}-2uv\Phi_{xy}+(a^2-v^2)\Phi_{yx}=0 \qquad (1)$$

or the equation for the conservation of mass

$$\frac{\partial}{\partial x}(\rho u)+\frac{\partial}{\partial y}(\rho v)=0 \qquad (2)$$

It is believed that difference approximations to the conservation law, Eq. (2), provide a better representation of shock waves in spite of the fact that in certain cases a better agreement between experiment and theory is found when applying the nonconservative form, Eq. (1). The results reported here were obtained with the fully conservative scheme.

The inviscid calculations are carried out in a computational plane obtained by conformally mapping the airfoil into a unit circle. The solution is established by employing a sequence of meshes using Jameson's accelerated iterative method[3] to speed up convergence. The viscous wake is represented by a semi-infinite parallel displacement body extending downstream of the trailing edge.[4]

Boundary-Layer Theory

For the boundary-layer computations Rotta's integral dissipation method[5] is employed. This method is based on simultaneously integrating the von Kármán momentum equation

$$\frac{d\Theta}{dx}+\Theta\left[\frac{H+2}{U_e}\frac{dU_e}{dx}+\frac{1}{\rho_e}\frac{d\rho_e}{dx}\right]=\frac{c_f}{2} \qquad (3)$$

and the energy equation

$$\frac{d\Theta^*}{dx}+\Theta^*\left[\frac{3}{U_e}\frac{dU_e}{dx}+(2-\gamma)\frac{1}{\rho_e}\frac{d\rho_e}{dx}\right]=c_D \qquad (4)$$

These equations are derived assuming adiabatic wall conditions and constant static pressure across the boundary layer.

In order to solve the preceding equations additional relations for the shape factor H, the skin friction coefficient c_f, and the dissipation coefficient c_D, must be given. A relation for the shape factor is derived from the power law velocity profile, the skin friction coefficient is determined using the well-known Ludwieg-Tillmann formulation, and for the dissipation coefficient an extended form of the dissipation law based on Nash's equilibrium boundary-layer relation that accounts for upstream history effects is utilized.[5]

Shock/Boundary-Layer Interaction Theory

To solve the transonic interaction problem for non-separating turbulent flow, i.e., for shock upstream Mach numbers of $M_1 \leq 1.3$, in the Reynolds number range of $Re \approx 10^6$ to 10^8, a nonasymptotic triple deck disturbance flow model is employed.[6] The model, Fig. 1, is comprised of an upper mixed flow region outside the boundary layer consisting of an incoming potential supersonic flow in region 1 and a subsonic potential flow in region 3 separated by a given shock discontinuity. Below these regions is a doubly-infinite nonuniform boundary-layer region (region 2) that contains a

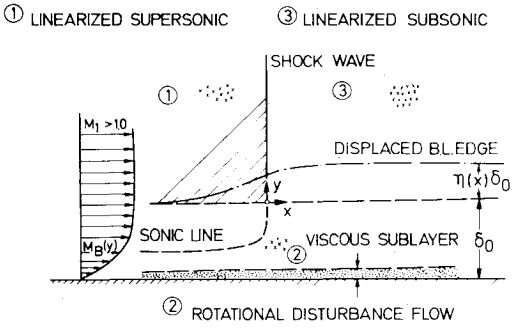

Fig. 1 Model of shock/boundary-layer interaction.

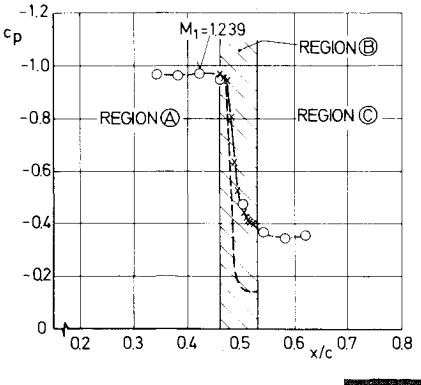

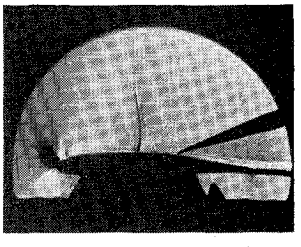

Fig. 2 Shock jump relations.

highly rotational, mixed transonic linear disturbance flow. Near the wall exists a viscous disturbance sublayer that contains the upstream influence and the skin friction perturbation.

An approximate analytic solution is obtained by assuming linearized disturbances ahead of and behind the nonlinear shock jump. The shock itself is taken as a simple discontinuity across which the Hugoniot shock jump relations are satisfied. To simplify the problem the shock jump conditions are only imposed at the boundary-layer edge neglecting the details of the subsequent shock penetration into the underlying nonuniform flow region.

The resulting equations are solved by operational methods. For the input required to start the interaction code and the properties calculated by the code, the reader is referred to the next section.

The normal shock jump relation contained in the original version of the interaction code generally overpredicts the surface pressure rise observed experimentally in transonic airfoil flow, Fig. 2. This is a result of the viscous layer causing the shock to be oblique in the vicinity of the airfoil surface. The normal shock relation, therefore, was replaced by the shock jump condition for maximum stream deflection. Here, the shock angle Θ is a function of the shock upstream Mach number only[7]:

$$\sin^2\Theta_{\delta_{\max}} = \frac{1}{4\gamma M_1^2}\{(\gamma+1)M_1^2-4 + \sqrt{(\gamma+1)[(\gamma+1)M_1^4+8(\gamma-1)M_1^2+16]}\} \quad (5)$$

With the shock angle given, the postshock Mach number M_2 and, hence, the shock jump

$$\frac{\Delta p}{p_1} = \left[1+\frac{\gamma-1}{2}M_1^2\right]^{\gamma/(\gamma-1)}\left[1+\frac{\gamma-1}{2}M_2^2\right]^{\gamma/(1-\gamma)} - 1 \quad (6)$$

can be determined. It should be noted that using the shock angle for maximum stream deflection can only be considered an approximation since the shock angle is likely to depend on the thickness of the incoming boundary layer. We are investigating this matter further.

Coupling

The viscous flow analysis is carried out by adding the displacement thickness to the geometric airfoil contour and performing the inviscid computation for the effective airfoil shape. The displacement thickness is obtained by the coupled boundary layer/shock boundary-layer interaction code (BSBI-code).

The domains of application of the two methods involved in computing the displacement thickness and other boundary-layer properties are shown in Fig. 3. For a given pressure distribution regions A and C are covered by boundary-layer theory. In region A the computation stops upstream of the shock providing the boundary-layer parameters necessary to start the interaction code, i.e., the local Reynolds number based on displacement thickness $Re_{\delta_1^*}$, and the shape factor H. Shock upstream Mach number and shock location are taken from the pressure distribution which is given either by experiment or inviscid theory. In region B the interaction code determines the displacement thickness, the shape factor and the skin friction coefficient, together with the surface pressure distribution due to shock impingement.

The input required to reinitiate the boundary-layer computation in region C, Fig. 3, is the momentum thickness Θ, and the energy thickness Θ^*. Since the interaction theory in its present form does not provide the energy thickness explicitly, Θ^* at the interface between regions B and C is determined from the given parameters H and δ^* as follows. There exists for flow with pressure gradients a unique relation between the shape factors $H=\delta^*/\Theta$ and $\bar{H}=\Theta^*/\Theta$ which for a certain class of power law profiles has the form

$$\bar{H}_i = 4.0H_i/(3H_i-1) \quad (7)$$

with the subscript i referring to incompressible flow.[8] In the present context the dependence of $\bar{H}$ on H downstream of a shock in transonic airfoil flow is needed. Results from the boundary-layer measurements described subsequently were, therefore, evaluated and a semiempirical relation based on Eq. (7), viz.,

$$\bar{H} = 1.26H/(H-0.39)+0.26/H \quad (8)$$

established. This relation allows the determination of the energy thickness Θ^* from the known quantities. It can be seen in Fig. 4 that Eq. (8) in its incompressible form (data points evaluated from u profiles) agrees quite well with Eq. (7) and other semiempirical relations[8,9] derived for incompressible flow.

It should be noted that the applicability of Eq. (8) is restricted to the immediate postshock region since the relation between the shape factors is—if only weakly—dependent on Mach number. Considering the accuracy with which Θ^* must be determined we found that the δ^* distribution downstream of the shock is much more sensitive to the starting value of δ^* than it is to the corresponding Θ^* and that, if δ^* was given with sufficient accuracy, essentially no error was introduced by applying the empirical relation of Eq. (8). With the initial values given, the boundary-layer computation in region C, Fig. 3, can now be completed.

The inviscid computation for the airfoil plus displacement surface starts with an initially assumed analytically modeled displacement thickness distribution generally of the form

$$\frac{\delta^*}{c} = \sum_k C_k\left(\frac{x}{c}\right)^{E_k} \quad (9)$$

with the initial values of C_k and E_k based on experience. Subsequently, the pressure distribution calculated after a certain prescribed number of iterations by the inviscid code is used as input to the boundary layer/shock boundary-layer interaction code which determines a new displacement surface. The latter is analytically approximated by Eq. (9) smoothing over the more sudden change in displacement thickness due to shock impingement. This smoothing has, of course, only a local effect since the change in boundary-layer properties across the shock has already been transmitted to the trailing edge by the preceding calculation. In approximating the computed displacement surface, usually three to four terms in the series represented by Eq. (9) are sufficient. The coefficients and exponents of the equation are

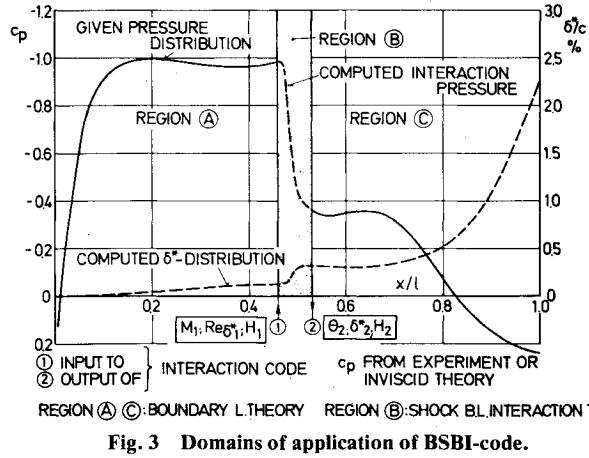

Fig. 3 Domains of application of BSBI-code.

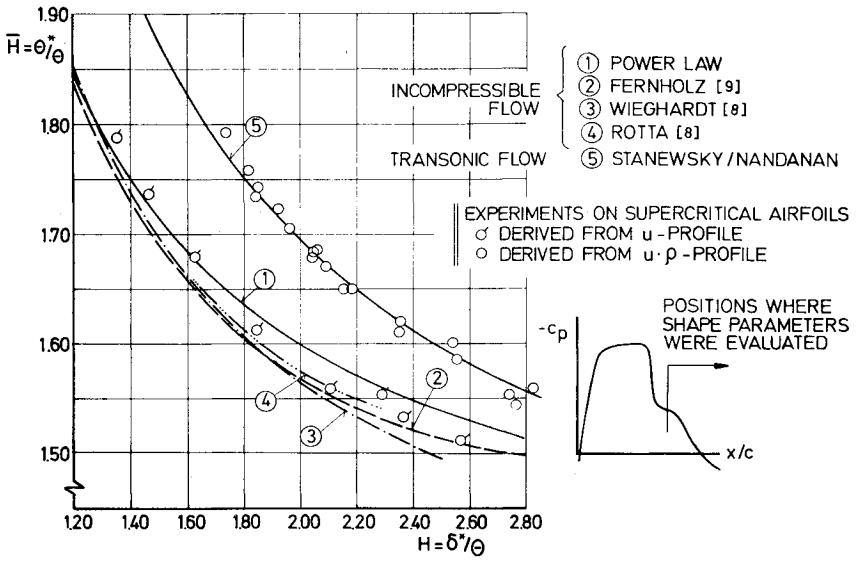

Fig. 4 Relations between shape factor H and $\bar{H}$.

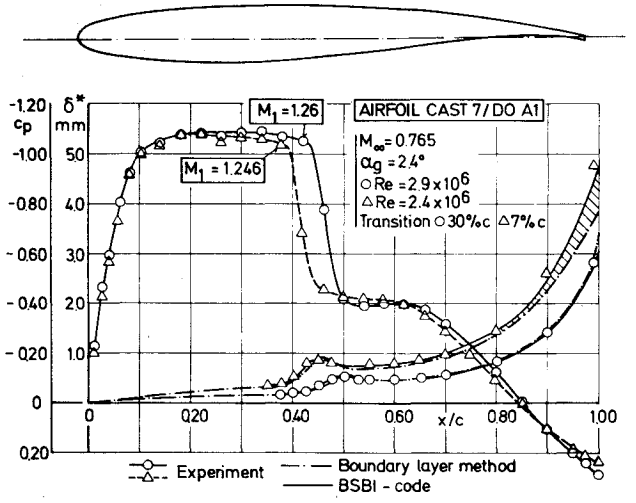

Fig. 5 Comparison of δ^* distributions obtained by experiment, boundary-layer code, and BSBI-code; airfoil CAST 7/DOA1.

determined with the aid of the slope of the calculated distribution at three to four prominent locations along the chord, such as, for instance, the trailing edge.

The new effective airfoil shape is obtained by adding the approximated δ^* distribution to the airfoil contour and repeating the inviscid computation. This procedure continues until the desired agreement between added and subsequently computed displacement thickness is achieved. With a proper initial guess, this generally takes three iterative steps.

Experimental Investigation

Results from the theory just described are compared to experimental data from boundary-layer and surface pressure measurements. The former were carried out on three supercritical airfoils having different characteristics in the pressure distribution. The freestream conditions were such that the local shock upstream Mach number—representative of the shock strength—on the upper surface varied between $M_1 = 1.23$ and 1.40 at Reynolds numbers between $Re = 2 \times 10^6$ and 3.5×10^6. The initial boundary-layer condition was, in addition, changed by varying the transition strip location. Besides the boundary-layer measurements, surface pressure and wake measurements were conducted on these airfoils testing one at Reynolds numbers up to $Re = 31 \times 10^6$ in the Lockheed transonic wind tunnel (CFWT).[10]

The boundary-layer and flowfield measurements were carried out in the 1×1-m transonic wind tunnel of the DFVLR-AVA Göttingen.[11] This tunnel is equipped with a 6%-open perforated test section with holes inclined 30 deg to the flow direction. The models generally had a chord length $c = 200$ mm and spanned the entire width of the test section. The relatively large span/chord ratio essentially eliminated side wall effects up to freestream conditions for total separation.

The boundary-layer probe employed consisted of a 0.15-mm fishmouth type pitot probe, a cone-cylinder static probe, and a directional probe made of two tubes cut-off under 45 deg.[12] To obtain velocity and density distributions in the boundary layer from the measured pitot and static pressures it was assumed that the total temperature is constant across the viscous layer. The boundary-layer integral parameters were determined by integration after having added to the measured data points, where applicable, i.e., generally in the thin boundary layer upstream of the shock, the laminar sublayer. The skin friction coefficient was determined by a modified Ludwieg-Tillmann formulation using the shape factor H_i derived from the measured u profiles as input.[12]

The transonic airfoil sections used in this investigation are designated CAST-7/DOA1 and CAST 10-2/DOA2[13] and Va 2.[14] The geometry of the airfoils is shown together with the results in the respective figures.

Results

The presentation and discussion of the results is divided into two parts, the first part discussing results obtained by the combined boundary-layer/shock boundary-layer interaction code for given experimental pressure distributions, the second part concerned with results from the complete viscous/inviscid method. In all instances comparisons with experimental data are presented.

Boundary-Layer Development

The boundary-layer development can be affected severely by the shock and the sustained adverse pressure gradients over the rear part of the airfoil upper surface. The question of main concern here is whether a conventional boundary-layer theory is capable of accurately predicting the change in boundary-layer parameters across the shock and the subsequent boundary-layer development down to the trailing edge.

Figure 5 shows the experimental and theoretical displacement thickness distribution, i.e., the parameter mainly felt by the outer inviscid flow, over the upper surface

of the airfoil CAST 7/DOA1 for different initial boundary-layer (displacement) thicknesses. In the experiments the difference in the initial δ^* was obtained by placing a transition strip at 7 and 30% c, respectively. The higher Reynolds number in the case of the latter was chosen to ensure that transition really occurred at the location of the strip. The theoretical δ^* distributions were obtained by 1) utilizing only boundary-layer theory and 2) employing the coupled boundary-layer/shock boundary-layer interaction code. Input was the experimental pressure distribution.

It can be seen that for the thin initial boundary layer—and the somewhat higher Reynolds number—the boundary-layer code is able to predict quite well the experimentally determined jump in displacement thickness due to the shock and the δ^* distribution between shock and trailing edge, Fig. 5. Considering the thicker initial boundary layer, the boundary-layer code overpredicts the jump in displacement thickness due to the shock; then underpredicts the decrease in δ^* due to the relaxed pressure gradient immediately downstream of the shock; and, starting with a value that is too low (although, as it seems, not by much), fails to predict the downstream development, appreciably underestimating the experimental value at the trailing edge. This must have a serious effect on circulation and, hence, on the overall pressure distribution and lift.

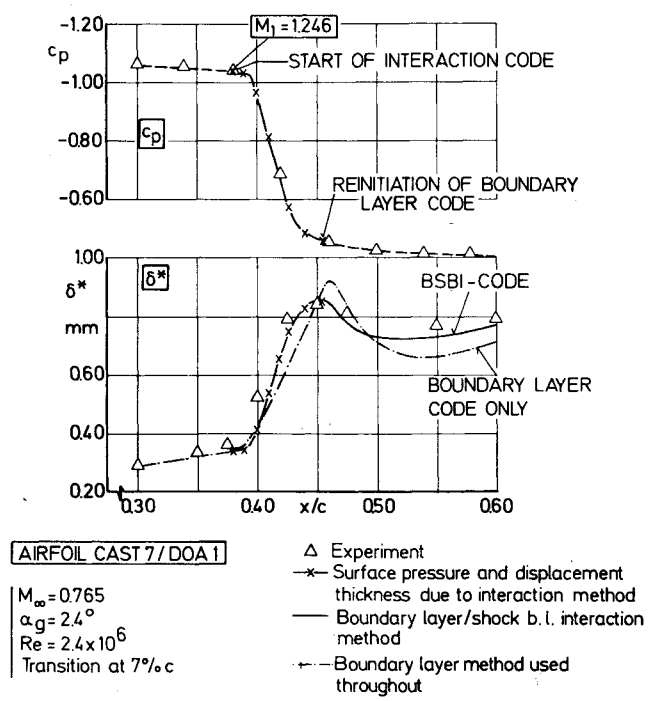

Fig. 6 Details in the interaction region; test case of Fig. 5 with thick initial boundary layer.

Applying the BSBI-code to the case of the thick initial boundary layer, one sees that the experimentally determined boundary-layer development throughout the interaction region and down to the trailing edge is quite well predicted. There is a marked improvement in the interaction region, as well as downstream, over the results obtained by utilizing boundary-layer theory throughout.

A closer look at details in the interaction region, Fig. 6, indicates that the interaction code commencing its computation at $x/c = 0.38$ gives results in very close agreement with the experimental interacting surface pressure and displacement thickness distribution. The slight underprediction of the experimental data in the plateau region by the BSBI-code could be due to a value at reinitiation slightly higher than the experimental data point. Note the large discrepancy between experiment and theory in the plateau region when the conventional boundary-layer code is used throughout the interaction region.

The δ^* distributions just discussed indicate why it seems important to determine the change in boundary-layer properties due to a shock wave with a high degree of accuracy. Small differences occurring immediately downstream of the interaction region are being amplified by the subsequent adverse pressure gradients resulting in large differences at the trailing edge. This must have appreciable consequences for the prediction of the overall pressure distribution and lift.

The amplification of initially small differences is likely to be dependent on the severity of the rear adverse pressure gradients. Rear adverse pressure gradients are slightly more severe on the airfoil CAST 10-2/DOA2 than on CAST 7/DOA1. The comparison of displacement thickness distributions given in Fig. 7 for the airfoil CAST 10/DOA2 and an initially thick boundary layer shows that here using the boundary-layer code throughout results in a larger discrepancy between theory and experiment, particularly in the trailing-edge region, than in the corresponding CAST 7/DOA1 case. Properly accounting for the shock/boundary-layer interaction again quite well predicts the experimentally determined δ^* distribution.

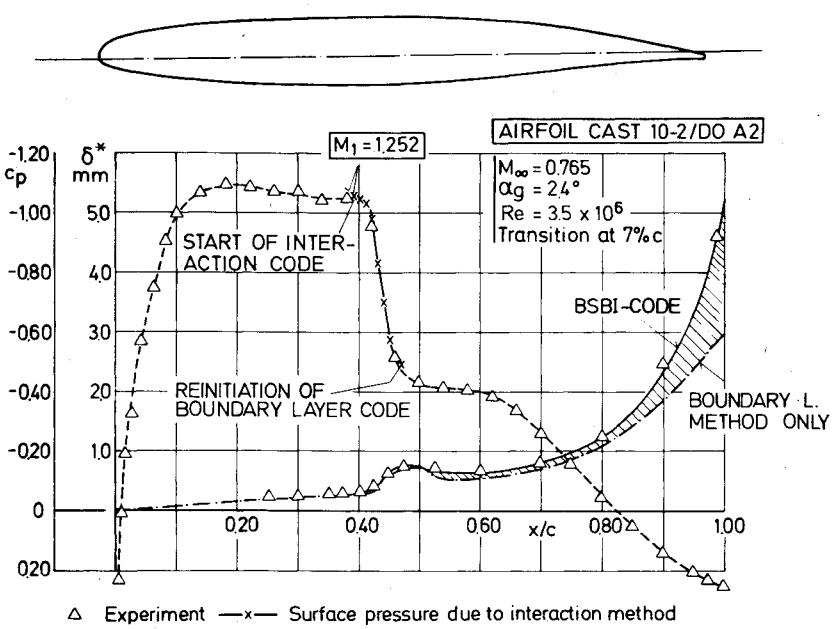

Fig. 7 Comparison of δ^* distributions obtained by experiment, boundary layer code, and BSBI-code; airfoil CAST 10-2/DOA2.

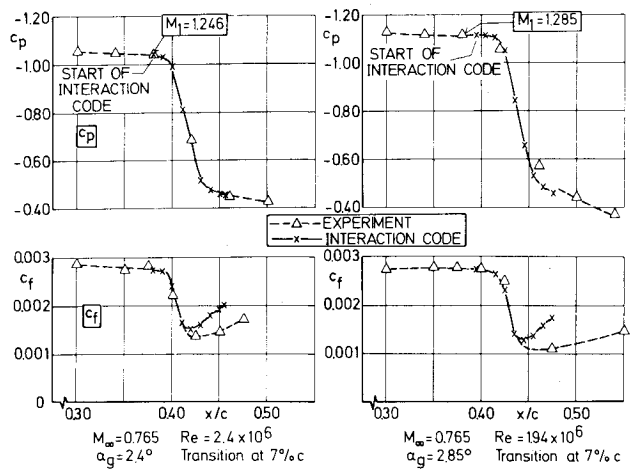

Fig. 8 Comparison of experimental and theoretical skin friction distributions.

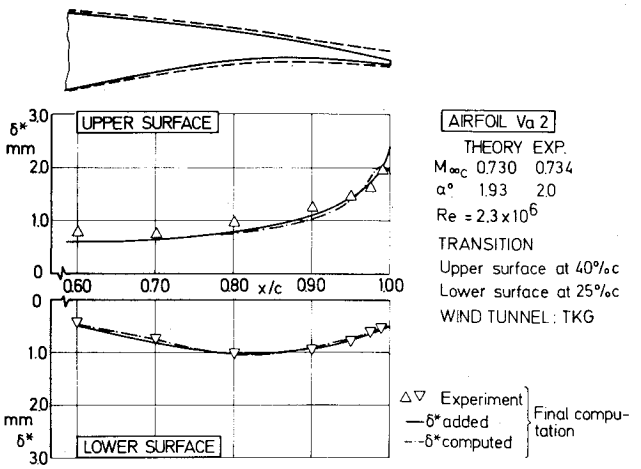

Fig. 10 Theoretical and experimental displacement thickness distributions: airfoil Va 2 (test case of Fig. 9).

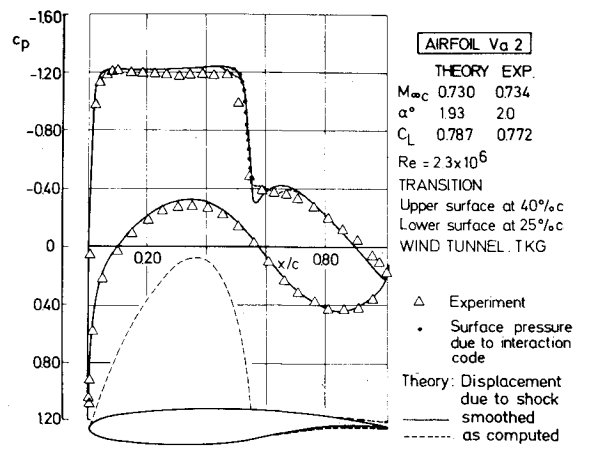

Fig. 9 Theoretical and experimental pressure distributions; airfoil Va 2.

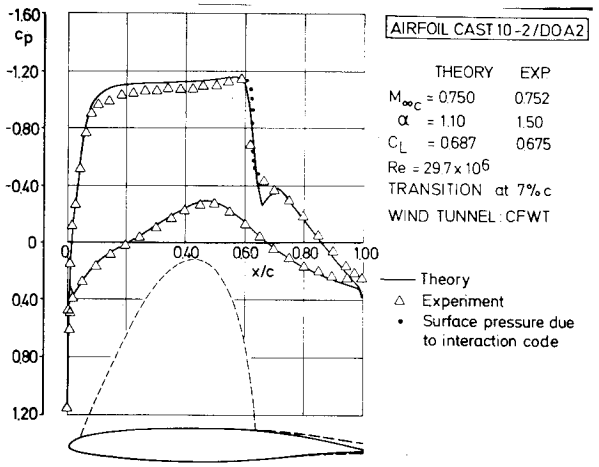

Fig. 11 Theoretical and experimental pressure distributions; airfoil CAST 10-2/DOA2.

The agreement between results obtained with the BSBI-code and experimental data remained good up to a shock upstream Mach number of $M_1 \approx 1.30$. For this Mach number the boundary-layer method indicated, contrary to the experimental results and in spite of smearing the pressure rise in the interaction region, separation and terminated the computation.

Before concluding the part concerned with the boundary-layer development it is thought necessary to briefly compare theoretical and experimental skin friction coefficients in the interaction region. The skin friction coefficient is a viscous parameter well suited to indicate (at least in two-dimensional flow) the onset of separation. As Fig. 8 shows, the drop in skin friction due to the shock and the location of the minimum in c_f observed experimentally are quite well predicted by the interaction theory with only a slight difference in the magnitude of c_f at the location of the minimum. Downstream of the minimum the interaction code overpredicts the experimental data. We are still investigating the cause for this discrepancy. Note that the skin friction does not enter the overall viscous computation.

Overall Flow Development

In the previous subsection it was shown that it is necessary to properly account for the shock/boundary-layer interaction in order to predict accurately the boundary-layer development down to the trailing edge. Here, results obtained for two airfoils by applying the present viscous/inviscid method to the analysis of supercritical flow with shock waves are discussed.

The first airfoil considered, viz., the Va 2, is a rear-loaded airfoil with a moderately peaky pressure distribution at the design point. Figure 9 compares theoretical and experimental c_p distributions, the latter measured in the 1×1-m TKG of the DFVLR, for a freestream Mach number $M_{\infty c} \approx 0.734$ and an angle of attack of $\alpha \approx 2.0$ deg. Transition in both experiment and computation was fixed at 40% c on the upper and 25% c on the lower surface. The experimental freestream conditions are corrected for wall interference effects. The correction factors were determined by comparison with results from the transonic wind tunnel Braunschweig (TWB) of the DFVLR for which zero blockage and only minor lift interference corrections are required.[15]

The experimental pressure distribution and the theoretical results obtained by the fully conservative scheme employing a mesh size of 256×64 are in good agreement, Fig. 9. The overprediction of the shock jump by the inviscid method in the case of the smoothed δ^* distribution is believed to be a result of just that, smoothing. Including the local change in displacement thickness as it was determined by the interaction code gives a shock jump, as is indicated by the dashed line in Fig. 9, in close agreement with experiment. Here, the small irregularities in the pressure distribution upstream and downstream of the main pressure rise are probably due to the conformal mapping of the effective airfoil contour.

The displacement thickness distribution that was 1) added to obtain the effective airfoil contour for the final computation of the c_p distribution of Fig. 9 and 2) recomputed by the BSBI-code with this pressure distribution as input is

compared in Fig. 10 with experimental data. One can see that on the lower surface there is excellent agreement in the displacement thickness distributions reflecting the good agreement in the corresponding c_p distributions (Fig. 9). The same holds for the upper surface except for the last 1% of the chord. Here, the displacement thickness computed with the final pressure distribution shows a slight decrease, contrary to the added and the experimental δ^*. This, of course, is due to the decrease in the corresponding theoretical pressure distribution, the latter possibly a result of not correctly treating the trailing edge interaction. Note that the displacement thickness added over the last 1% of the chord will be, in general (following experimental observations), of the form given by the full line in Fig. 10.

The second test case concerns the airfoil CAST 10-2/DOA2 for which demands on the boundary layer are more severe than in the preceding case, Fig. 11. (Note that the trailing edge angle of this airfoil is about 15 deg.) The experimental results were obtained in the Lockheed CFWT at a Reynolds number of $Re \approx 30 \times 10^6$ and transition fixed at 7% c. The theoretical results were again computed with the fully conservative scheme but using a mesh size of 128×32. The c_p distributions are in good agreement; however, there is a difference in the angle of attack of 0.4%. This may be attributed to the fact that the angle-of-attack correction, established as described earlier, does not account fully for conditions in the Lockheed CFWT.

Further comparisons of experimental and theoretical pressure distributions, the latter obtained by the present and other theoretical methods, are presented in Ref. 16.

Concluding Remarks

In the present approach to transonic airfoil flow analysis an analytical solution for near-normal shock wave/boundary-layer interaction was embedded as a module within a state-of-the-art boundary-layer/inviscid computation code. A brief account of the theory and the elements involved was given. Results obtained with 1) the combined boundary-layer/shock boundary-layer interaction code and 2) with the complete viscous/inviscid method were compared to corresponding experimental data from boundary-layer and surface pressure measurements. The following conclusions may be drawn from these comparisons.

1) It is generally necessary to include a physically correct treatment of the shock/boundary-layer interaction since the change in boundary-layer properties due to the interaction must be known to a high degree of accuracy not provided by conventional boundary-layer theory. The accuracy is required because small differences in the boundary-layer properties immediately downstream of the interaction are being amplified by the rear adverse pressure gradients leading to large differences at the trailing edge with all its consequences to the prediction of the overall pressure distribution and lift and drag.

2) There is some evidence that in the case of an initially thin boundary layer and other favorable circumstances a boundary-layer method using artificial smearing of the pressure rise may be able to predict the changes in boundary-layer properties across a shock with sufficient accuracy. However, relying on this approach can lead to large errors in the design and analysis of transonic airfoils.

Acknowledgments

The authors want to express their gratitude to Dr. H. Sobieczky for many constructive suggestions, such as the replacement of the normal shock jump relation with the one for maximum stream deflection, during the course of the work reported here.

References

[1] Sirieix, M., Delery, J., and Stanewsky, E., "High Reynolds Number Boundary-Layer Shock-Wave Interaction in Transonic Flows—Cooperative Work Carried out at DFVLR and ONERA," *Proceedings of the Conference on Fluid Mechanics,* Rheinisch-Westfälische Technische Hochschule-Aachen, FRG, March 1980; also, *Lecture Notes in Physics,* Vol. 148, Springer-Verlag, Berlin, Nov. 1981, to be published

[2] Melnik, R. E., Chow, R., and Mead, H. R., "Theory of Viscous Transonic Flow Over Airfoils at High Reynolds Number," AIAA Paper 77-680, June 1977.

[3] Jameson, A., "Numerical Computation of Transonic Flow with Shock Waves," *Symposium Transsonicum II,* Springer-Verlag, Berlin, 1975, pp. 384-414.

[4] Bauer, F., Garabedian, P., Korn, D., and Jameson, A., *Supercritical Wing Sections II,* Springer-Verlag, Berlin, 1975.

[5] Rotta, J.-C., "Turbulent Boundary Layer Calculations with the Integral Dissipation Method," *Computation of Turbulent Boundary Layers - 1968 AFOSR-IFP Stanford Conference,* Vol. I, p. 177.

[6] Inger, G. R. and Mason, W. H., "Analytical Theory of Transonic Normal Shock-Turbulent Boundary-Layer Interactions," *AIAA Journal,* Vol. 14, Sept. 1976, pp. 1266-1272.

[7] "Equations, Tables, and Charts for Compressible Flow," NACA 1135, 1953.

[8] Schlichting, H., *Boundary Layer Theory,* 4th Ed., McGraw-Hill Book Co. Inc., New York, 1960, p. 574.

[9] Fernholz, H., "Semi-Empirical Laws for Computation of Turbulent Boundary Layers by the Method of Integral Relations," *Ingenieur Archiv,* Vol. XXXIII, 1963/64, pp. 384-395.

[10] Stanewsky, E., Puffert, W., and Müller, R., "Comparison of Wind Tunnel Wall Interferences in Several Transonic Tunnels," *Proceedings of the Conference on Effects of Wind Tunnel Flow on Experimental Results,* DGLR-Fachausschuss 3.1. Hydro-, Aero- and Gasdynamics, Göttingen, Feb. 6-7, 1979, Paper 1-3.

[11] Hottner, Th. and Lorenz-Meyer, W., "The Transonic Wind Tunnel of the Aerodynamische Versuchsanstalt Göttingen," *DGLR-Jahrbuch 1968,* pp. 235-244.

[12] Stanewsky, E. and Thiede, P., "Boundary Layer and Wake Measurements in the Trailing Edge Region of a Rear-Loaded Transonic Airfoil," *Proceedings of the 4th US-FRG-Meeting on Viscous and Interacting Flow Field Effects,* German Government-Rept. BMVg-FBWT 75-31, pp. 31-35.

[13] Kühl, P. and Zimmer, H., "Design of Airfoils for Transport Aircraft with Improved High Speed Characteristics," DORNIER GmbH, Friedrichshafen, FRG, Rept. 74/16B, 1974.

[14] Hilbig, R., "Design of the Transonic Airfoil Va 2," German Government Rept. BMFT-ZKP LFK 7511, Ergebnisbericht Nr. 7, 1977.

[15] Stanewsky, E., Puffert, W., and Müller, R., "The DFVLR Transonic Wind Tunnel Braunschweig: Calibration Results for the Modified Test Section and Results for the Airfoil CAST 7/DOA1," DFVLR Rept. IB 151-77/10, 1977.

[16] Stanewsky, E., Nandanan, M., and Inger, G. R., "The Coupling of a Shock Boundary Layer Interaction Module with a Viscous-Inviscid Computation Method," *Proceedings of the Symposium on Computation of Viscous-Inviscid Interactions,* AGARD CPP 291, Sept./Oct. 1980, Paper 4.